Neuropilin-1-Targeted Gold Nanoparticles Enhance Therapeutic Efficacy of Platinum(IV) Drug for Prostate Cancer Treatment

Anil Kumar,[†,‡] Shuaidong Huo,[†] Xu Zhang,[†] Juan Liu,[†] Aaron Tan,[§] Shengliang Li,[†] Shubin Jin,[†] Xiangdong Xue,[†] YuanYuan Zhao,[†] Tianjiao Ji,[†] Lu Han,[†] Hong Liu,[‡] XiaoNing Zhang,[⊥,*] Jinchao Zhang,[∥,*] Guozhang Zou,[†] Tianyou Wang,[#,*] Suoqin Tang,[⊗] and Xing-Jie Liang[†,*]

[†]CAS Key Laboratory for Biomedical Effects of Nanomaterials and Nanosafety, National Center for Nanoscience and Technology, Beijing, 100190, People's Republic of China, [‡]Beijing Institute of Nanoenergy and Nanosystems, Chinese Academy of Sciences, 30 Xueyuan Road, Haidian, Beijiing, 100083, People's Republic of China, [§]Centre for Nanotechnology & Regenerative Medicine, UCL Division of Surgery & Interventional Science, University College London (UCL), London, United Kingdom, [⊥]Department of Pharmacology and Pharmaceutical Sciences, School of Medicine, Tsinghua University, Beijing, 100084, People's Republic of China, [∥]College of Chemistry & Environmental Science, Chemical Biology Key Laboratory of Hebei Province, Hebei University, Baoding, People's Republic of China, [#]Capital Institute of Pediatrics, No. 2, Yabao Road, Chaoyang District, Beijing, 100020, People's Republic of China, and [⊗]Department of Pediatrics, The General Hospital of People's Liberation Army, No. 28, Fuxing Road, Haidian District, Beijing 100853, People's Republic of China

ABSTRACT Platinum-based anticancer drugs such as cisplatin, oxaliplatin, and carboplatin are some of the most potent chemotherapeutic agents but have limited applications due to severe dose-limiting side effects and a tendency for cancer cells to rapidly develop resistance. The therapeutic index can be improved through use of nanocarrier systems to target cancer cells efficiently. We developed a unique strategy to deliver a platinum(IV) drug to prostate cancer cells by constructing glutathione-stabilized (Au@GSH) gold nanoparticles. Glutathione (GSH) has well-known antioxidant properties, which lead to cancer regression. Here, we exploit the advantages of both the antioxidant properties and high surface-area-to-volume ratio of Au@GSH NPs to demonstrate their potential for delivery of a platinum(IV) drug by targeting the neuropilin-1 receptor (Nrp-1). A lethal dose of a platinum(IV) drug functionalized with the Nrp-1-targeting peptide (CRGDK) was delivered specifically to prostate cancer cells *in vitro*. Targeted peptide ensures specific binding to the Nrp-1 receptor, leading to enhanced cellular uptake level and cell toxicity. The nanocarriers were themselves nontoxic, but exhibited high cytotoxicity and increased efficacy when functionalized with the targeting peptide and drug. The uptake of drug-loaded nanocarriers is dependent on the interaction with Nrp-1 in cell lines expressing high (PC-3) and low (DU-145) levels of Nrp-1, as confirmed through inductively coupled plasma mass spectrometry and confocal microscopy. The nanocarriers have effective anticancer activity, through upregulation of nuclear factor kappa-B (NF-κB) protein (p50 and p65) expression and activation of NF-κB-DNA-binding activity. Our preliminary investigations with platinum(IV)-functionalized gold nanoparticles along with a targeting peptide hold significant promise for future cancer treatment.

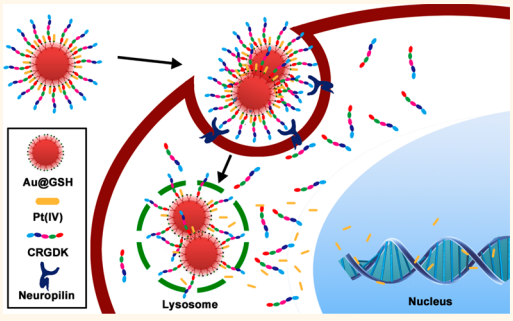

KEYWORDS: platinum(IV) drug complex · glutathione-stabilized gold NPs (Au@GSH) · targeted drug delivery systems (TDDSs) · neuropilin-1 (Nrp-1) receptor · NF-κB mechanism

Cisplatin, a well-known chemotherapeutic also known as a platinum(II) drug, is one of the most clinically successful platinum-based anticancer drugs and has been used in 70% of all tumor therapies, including breast and prostate cancer.[1,2] Significant efforts have been undertaken to enhance anticancer activity of platinum-based drugs as well as overcome adverse side effects such as peripheral neuropathy, high-frequency hearing loss, and nephrotoxicity associated with these drugs. Recently, a new series of platinum-based compounds such as platinum(IV) have been gaining attention for their anticancer properties.[3] Indeed, many platinum series compounds have been synthesized and their anticancer activities examined.[4,5] Among them, platinum(IV) compounds have been reported to be potential anticancer agents.

Platinum(IV) drugs exhibit several advantages over the parent complex (cisplatin) for

* Address correspondence to drugman@mail.tsinghua.edu.cn (X.-N. Zhang), jczhang6970@163.com (J. Zhang), wangty999@sohu.com (T. Wang), liangxj@nanoctr.cn (X.-J. Liang).

Received for review August 26, 2013 and accepted April 14, 2014.

Published online April 14, 2014
10.1021/nn500152u

cancer treatment. Their high coordination number (six) enables fine-tuning of pharmacological properties such as reduction potential, lipophilicity, and kinetic stability.[6] Moreover, compared to platinum(II), platinum(IV) complexes have been reported to be inert compounds that can be administered at higher dosage levels to achieve increased antitumor efficacy without adverse side effects, thus opening up more possibilities for oral drug administration.[6−9]

A major challenge for improving anticancer treatments is to direct the therapeutic agent specifically to the tumor cells or tumor blood vessels, thus enhancing the efficacy of the treatment and decreasing undesirable side effects.[10,11] Therefore, application of targeted drug delivery system (TDDSs) is significant for reducing the undesirable side effects of anticancer drugs in healthy cells/organs, thereby improving the therapeutic efficacies.[10] Different strategies have been designed to achieve this goal. Gold nanoparticles (NPs) can be functionalized with a plethora of medically important components.[10] Moreover, gold NPs are widely considered as an ideal drug delivery platform, as they are known to be nontoxic and nonimmunogenic. Furthermore, they are easy to synthesize, and their high surface area increases drug density on the surface, allowing higher concentrations of a drug or indeed multiple drugs to be simultaneously loaded onto a single nanoparticle.[12] The unique physiochemical properties of gold NPs can also trigger drug release at remote sites, creating a multipronged approach to destroying cancer cells.[13]

Currently, there are numerous reports that gold NPs, when used as drug carriers for cancer treatment, yield more favorable results compared to standard anticancer drug treatments.[14,15] Moreover, some studies suggested that gold NP-based drug delivery systems can circumvent multidrug resistance in cancer cells and increase the therapeutic index.[16,17] Recently tumor necrosis factor (TNF)-α-coated gold NPs, termed CYT-6091, have augmented the clinical significance of gold NPs. CYT-6091 was the first gold NP-based novel nanomedicine to undergo phase I clinical trials for advanced-stage cancer patients.[18] Several gold-based NP systems have already been approved for therapeutic use by the Food and Drug Administration (FDA),[10] with some in various stages of advanced clinical trials.[19]

During the development of metastatic tumors, cells can upregulate certain cell-surface receptors molecules and secreted factors, as well as express several oncogenic proteins primarily involved during embryonic development.[20] However, cancer cells often have similar characteristics to surrounding healthy tissue, making treatment more challenging. In such cases, ligands can be designed that have high specificity and affinity for receptors that are overexpressed on cancerous cells. Since the targeting ligands are generally presented on the outermost sector of the nanoparticle delivery system,[21] glutathione-stabilized gold (Au@GSH) nanoparticles were designed with a targeting moiety on the surface with the aim of selectively increasing cellular binding and internalization *via* receptor-mediated endocytosis (Scheme 1).

Neuropilin-1 (Nrp-1) plays a significant role during angiogenesis and vascular permeability.[22,23] Nrp-1 is a transmembrane glycoprotein that binds peptides with a C-terminal amino acid motif R/KXXR/K, called the CendR motif (found in semaphorin 3A, VEGF-A165, and iRG).[26] Binding of the CendR peptide to Nrp-1 mediates cell internalization and tissue penetration.[24] Nrp-1 is expressed by a large variety of tumors, including osteosarcoma, melanoma, lung cancer, brain tumor, colon cancer, pancreatic cancer, prostate cancer, breast cancer, myeloid leukemia, salivary adenoid cystic carcinoma, infantile hemangioma, ovarian neoplasm, and bladder cancer.[25,26] Nrp-1 has high affinity toward its cognate ligands, thereby enabling nanoparticles to penetrate into tumor cells and tissues.[27]

Thus, we assumed that introduction of a targeting peptide specific for Nrp-1 receptor may be a more effective way to increase the efficacy for tumor penetration of platinum(IV) drugs. We selected the CendR peptide ligand Cys-Arg-Gly-Asp-Lys (CRGDK), which binds the Nrp-1 receptor, as reported previously from our lab in relation to breast cancer treatment.[12,28]

Systematic evaluation of CRGDK as a target ligand for prostate cancer treatment has not been reported before. Therefore, in our study, the Nrp-1 receptor was selectively targeted to enhance delivery of a therapeutic drug such as platinum(IV) and achieve higher cytotoxic effects in prostate cancer cells. Theoretically, the receptor's (Nrp-1) presence on the cell surface should increase the binding affinity as well as the intake of CRGDK-functionalized NPs by the tumor cells.

In the present study, we have combined the properties of gold NPs stabilized with glutathione (Au@GSH) along with a platinum(IV) drug and the targeting peptide CRGDK into a single platform to create an effective TDDS for prostate cancer treatment. In the absence of targeting ligands, nanoparticles interact nonspecifically with cell membranes, which are not sufficient to achieve an optimal effect of a drug at the disease site.[27,29] Here we show that small Au@GSH NPs (5.2 nm) functionalized on the surface with platinum(IV) and CRGDK have effective targeting activity and demonstrate potent cytotoxicity against prostate cancer cells that overexpress Nrp-1 receptors.

RESULTS AND DISCUSSION

Synthesis and Characterization of Monodispersed GSH-Stabilized Gold Nanoparticles. In order to develop TDDSs based upon small gold NPs, we synthesized glutathione-stabilized gold NPs (Au@GSH) with a size of about 5.2 nm in diameter. The tripeptide glutathione is an

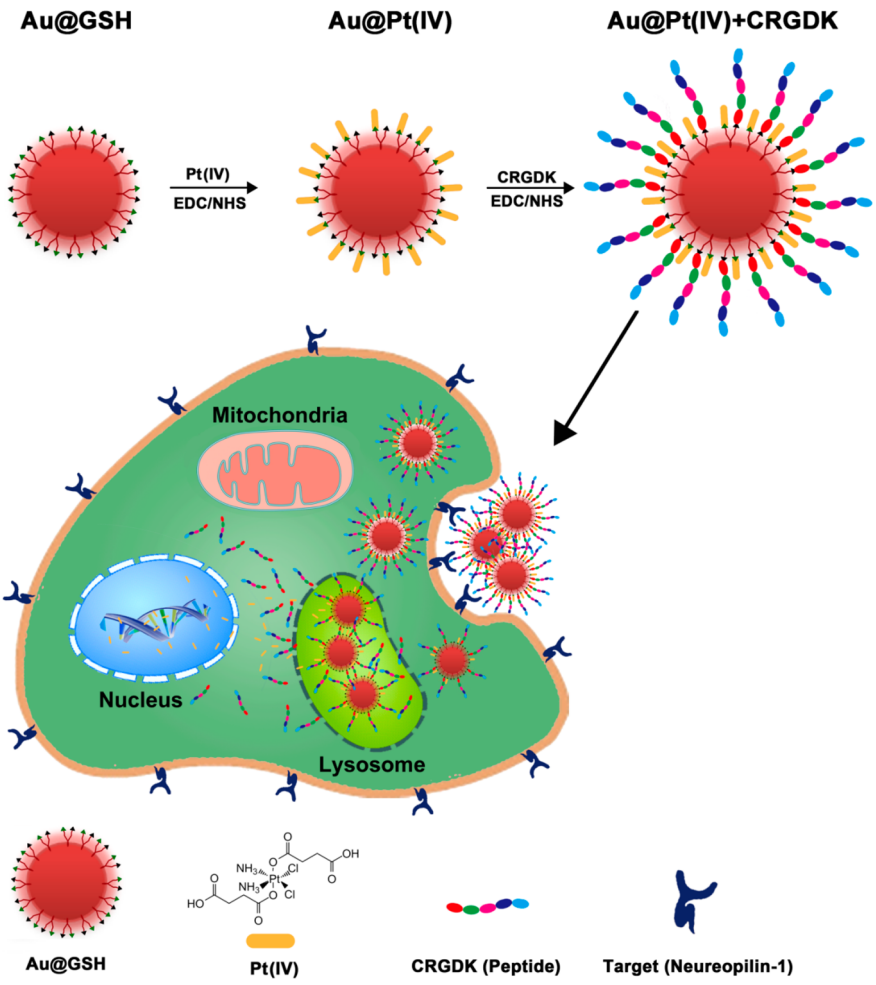

Scheme 1. (Upper part) Scheme for the functionalization of Au@GSH gold NPs with the chemotherapeutic drug Pt(IV) and the targeting peptide CRGDK for cancer treatment. (Lower part) Interaction between the neuropilin-1 receptor and the targeting ligand, which enhances intracellular entry and release of active cisplatin into the nucleus of human prostate cancer cells after endocytosis (receptor-mediated) of the Au@Pt(IV)+CRGDK delivery system.

important thiol-based antioxidant in cells, helping to neutralize reactive oxygen species (ROS) such as free radicals and thus inhibiting cancer progression[30] Glutathione-stabilized gold NPs have been previously used in material sciences, but have not been explored widely in the biomedical field. *In vivo* studies have recently shown that gold NPs modified with another thiol-bearing molecule, tiopronin, can cause serious side effects. These effects can be eliminated by adding poly(ethylene glycol) (PEG) to the surface of the NPs, but PEG reduces the therapeutic properties of the nanocarriers. In contrast, glutathione-stabilized small AuNPs (1.2 ± 0.9 nm) show good biocompatibility *in vivo* at concentrations up to 60 μM. They become localized to primary organs, from which they are eventually cleared. Thus, GSH appears to be a good alternative to PEG in the synthesis of gold NPs for therapeutic applications.[31]

In our study, GSH-stabilized small gold nanoparticles were directly prepared using glutathione as the protecting agent with sodium borohydride ($NaBH_4$) as the reducing agent (Scheme S1, Supporting Information). Due to the strong reducing power of GSH, simple mixing of a gold salt with GSH solution at room temperature spontaneously results in the formation of Au@GSH NPs. Moreover, GSH also acts as a stabilizer by forming "S−Au" coordination bonds with the NP surface. Characterization of NPs was performed through TEM, UV−vis spectroscopy, zeta potential measurements, and X-ray photoelectron spectroscopy (XPS).

Au@GSH NPs were found to be highly soluble in water and stable under physiological conditions such as in culture medium under the influence of electrostatic interaction of the surface charge of the nanoparticles. Transmission electron microscope (TEM) analysis revealed that the Au@GSH NPs had a small core size of 5.2 ± 0.7 nm in diameter with uniform dispersion (Figure 1a). The size of more than 100 NPs was measured, and the mean diameter was calculated to be 5.2 ± 0.7 nm (Figure 1b). UV−visible absorbance measurements of the Au@GSH NPs showed surface plasmon peak bands (λ_{max}) detectable at 527 nm (Figure 1c) as compared to citrate-stabilized (15 nm) gold NPs.[32] Zeta potential studies of the NPs in water showed a negative

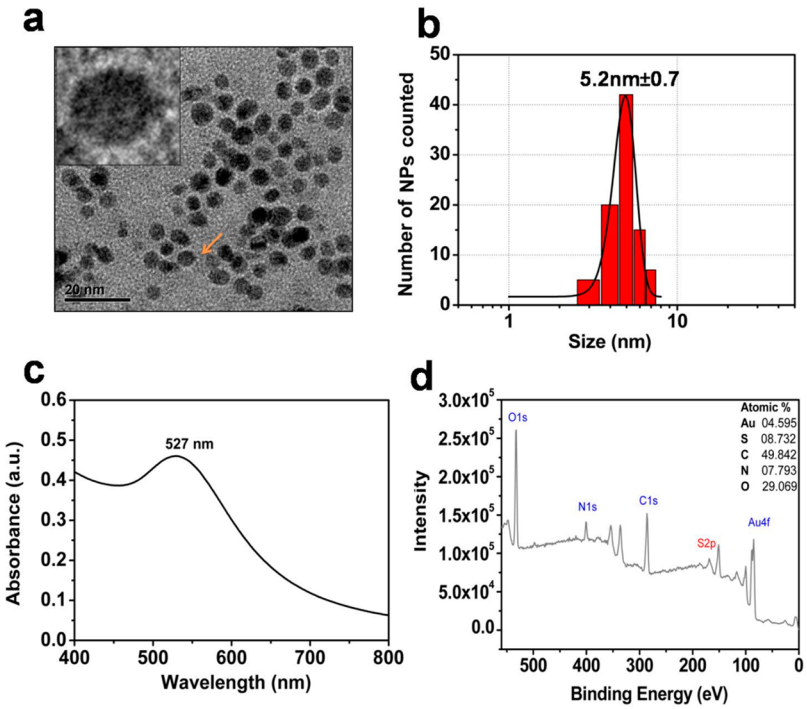

Figure 1. Characterization of glutathione-stabilized gold NPs (Au@GSH): (a) Typical TEM image of Au@GSH NPs in H_2O (scale bar 20 nm). The upper left panel shows the organic GSH layer stabilized on the surface of a small NP. (b) Size measurements of Au@GSH NPs. The histogram depicts the size of 100 particles analyzed. The mean diameter is 5.2 ± 0.7 nm. (c) UV−vis spectrum of the Au@GSH NPs, showing peak absorbance at a wavelength (λ) of 527 nm. (d) XPS study (elemental analysis) of Au@GSH NPs.

charge of −33.7 mV (Figure S1, Supporting Information). The XPS study shown in Figure 1d indicated that the molar ratio of "S" to "Au" in 5.2 nm Au@GSH NPs was 0.526, and the number of GSH molecules per NP was 4358. In addition, the surface density of GSH was calculated to be 27 for 5.2 nm Au@GSH NPs (the method used to calculate the number and surface density of GSH molecules per NP is given in the Supporting Information). The concentration and molecular weights of the particles were determined by calculating the gold atom concentration in accordance with inductively coupled plasma mass spectrometry (ICP-MS) measurements.[33]

Synthesis and Characterization of Platinum(IV) Complex 1 and Complex 2. A variety of platinum(IV) drug-based complexes have been developed, and their effects were studied in the last few decades, with some even entering clinical trials.[34,35] Some studies have indicated that the reduction potential of these platinum(IV) compounds is a very crucial factor in determining their antitumor properties/activities. Complex **2** was selected because it has an ideal reduction potential and is thus quite stable to traverse the bloodstream and reaches the tumor cells without premature decomposition compared to the parent complex. Moreover, complex **2** undergoes a positive shift in reduction potential (due to the acidic environment of the endosomes) and, thus, gets readily reduced to platinum(II) after entry inside the cells.[36] However, a critical challenge underlying the use of platinum(IV) drugs is that the latter needs to be protected against reduction before entering cancer cells. With this aim, we synthesized a platinum(IV) drug with the oxidation of cisplatin (also known as platinum(II)) in the presence of H_2O_2, to afford complex **1**, which bears two hydroxyl groups (Scheme 2) at its axial positions. Further succinic anhydride was used to react with the hydroxyl groups of complex **1** to obtain complex **2** (Scheme 2) and resulted in a free carboxyl group (COOH), capable of reacting with NH_2 groups for functionalizing the surface of the Au@GSH NPs by (*N*-(3-(dimethylamino)-propyl)-*N*-ethylcarbodiimide hydrochloride (EDC)/sodium *N*-hydroxysuccinimide (NHS) coupling. The complex **2** drug, also known as platinum(IV), was successfully synthesized with a high level of purity. The structure of complex **2** was confirmed by ESI-MS, FT-IR (Figures S3−S4, Supporting Information), and ^{1}H NMR (see Supporting Information for details).

Synthesis and Characterization of Drug- and Peptide-Functionalized Nanocarriers: Au@CRGDK, Au@Pt(IV), and Au@Pt(IV)+CRGDK. Recently, several platinum(IV) complex-based polymeric NP systems have been designed for drug delivery purposes and were found to be effective and successful for treating cancer cells both *in vitro* and *in vivo*.[37,38] However, very few studies have reported the use of gold NP-based platinum(IV) drug delivery for cancer therapy.[36,39] To our knowledge, this is the first report wherein gold NPs have been directly

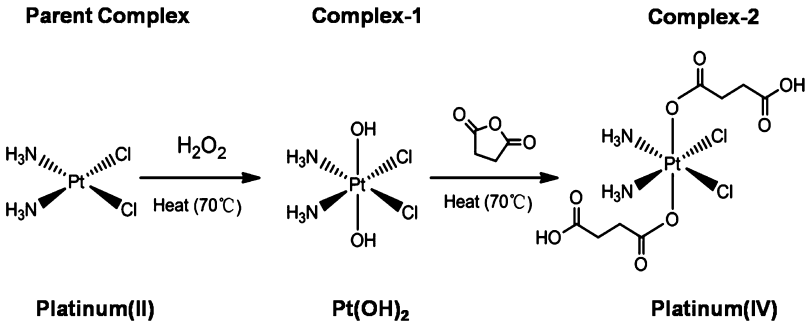

Scheme 2. Scheme for the synthesis of the platinum(IV) drug complex, showing the mechanism involved in modifying the axial ligands by succinic anhydride.

functionalized with a platinum(IV) drug along with a targeting peptide (CRGDK) without using external coating or ligand exchange and then employed to enhance cellular localization and therapeutic efficacy as a result of receptor-mediated endocytosis.

Our drug delivery system was designed to selectively target the Nrp-1 receptor to enhance delivery of therapeutic drug into cancerous cells and achieve higher cytotoxicity effects. Here, we functionalized the Au@GSH NPs with the platinum(IV) drug and the targeting peptide using two different procedures (see the Supporting Information for details).

A bicinchoninic acid (BCA) assay was performed to determine the exact quantity of peptide present on the surface of the Au@GSH NPs.[12] To confirm the amount of platinum(IV) drug loaded onto the NPs' surface, ICP-MS was performed.[40] The total amount of peptide and drug loaded onto the surface of the NPs was calculated in percentages as described in the Experimental Section, and the final concentration of platinum (Pt) was obtained in μg/mL. Finally, the amount of drug was converted into percentages, and molar concentrations were used for treating the cells.

Our quantification studies showed that in the case of the Au@CRGDK sample, CRGDK displayed 83% conjugation efficiency, while in the case of Au@Pt(IV)+CRGDK, almost the same amount of CRGDK (82.7%) was found to be conjugated against 78% of platinum(IV) drug, indicating a high level of conjugation efficiency. The amounts of drug and targeted peptide loaded into the surface of Au@GSH NPs were kept similar throughout the experiments described in this study.

To obtain a comprehensive characterization of the physicochemical properties of Au@GSH NP-functionalized products and their suitability for use *in vitro*, analyses were carried out using UV−visible spectroscopy, zeta potential measurements, agarose gel electrophoresis (to detect peptides on the NP surface), ICP-MS (to detect Pt in the solution), and XPS (to detect Pt on the surface of the NPs). The visible absorption spectrum can help to characterize physicochemical properties of NPs, *e.g.*, shape, size, monodispersion, and surface functionalization. UV−visible spectroscopy of the functionalized Au@GSH samples showed that the wavelength of the surface plasmon peak was increased compared to the surface plasmon peak (527 nm) of unconjugated Au@GSH NPs (Figure 2a). It is well known that the zeta potential of gold NPs mainly depends on surface functionalization. Significant changes in charge distribution were also observed in the drug- and CRGDK-functionalized samples (Figure 2b and Figure S1 in the Supporting Information), compared to NPs without any functionalization. The charge of Au@GSH NPs (−33.7 mV) was shifted in a positive direction (to −22.1 mV) upon conjugation with CRGDK hydrophilic peptide, indicating that CRGDK molecules are present on the gold NP's surface After functionalization of Au@GSH NPs with the platinum(IV) drug, the charge of the conjugated sample increased slightly to −25.7 mV, indicating the presence of platinum(IV) on the surface. Similarly, the charge of Au@Pt(IV)+CRGDK again shifted in the positive mode (−23.7 mV, close to Au@CRGDK), indicating the CRGDK presence on the Au@Pt(IV) NPs' surface.

We also attempted to detect the conjugation of functionalized Au@GSH NPs *via* agarose gel electrophoresis (Figure 2c). The samples were mixed with glycerol before loading onto the gel. Addition of glycerol did not cause aggregation of the samples. All functionalized nanocarriers produced a smear (Figure 2c lower) and had slow mobility compared to Au@GSH (unbound gold NPs), indicating the presence of peptide or drug on the surface of NPs, in agreement with previous reports.[41] Pt was detected by ICP-MS in solution and by XPS, confirming the presence of platinum(IV) on the surface of the NPs (Figure S5, Supporting Information).

Taken together, the above characterization studies demonstrated the successful synthesis and functionalization of Au@GSH NPs with drug and peptide. After synthesis the products were lyophilized and dried fully under vacuum and then dissolved in water for further experimental use.

Cytotoxicity of Functionalized Nanocarriers. The cytotoxic effects of Au@GSH NPs (unconjugated NPs), free drugs,

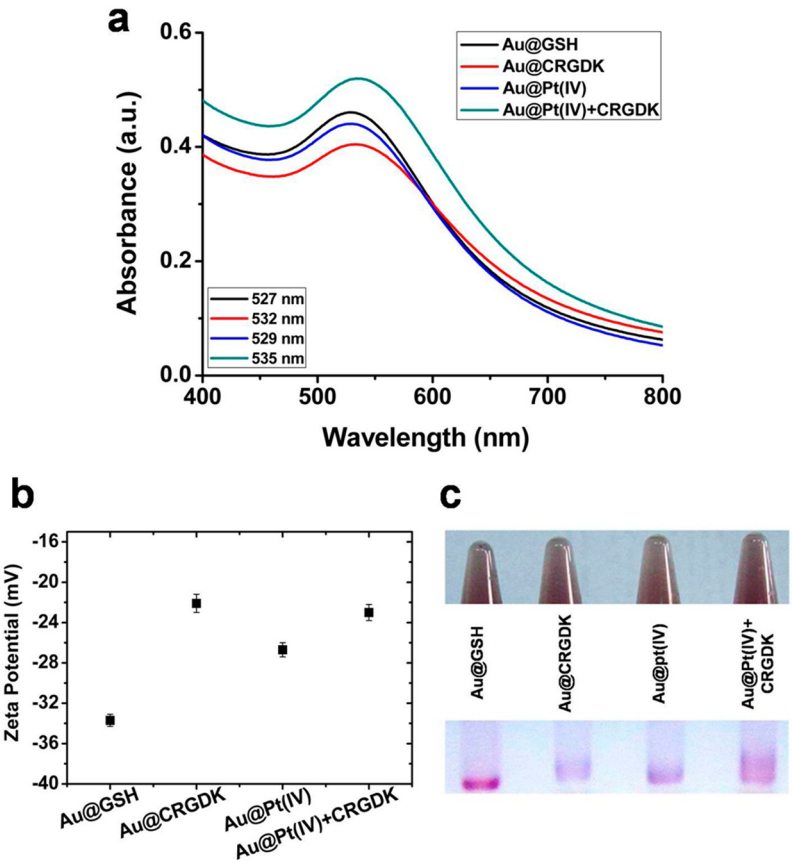

Figure 2. Characterization of Au@GSH NPs after functionalization with drug and peptide: (a) UV−vis spectra of the Au@GSH NPs functionalized with drug and peptide at wavelengths between 400 and 800 nm in pure water. The wavelength of the plasmon band peak increases after the Au@GSH NPs are surface-functionalized with drug and peptide. (b) The zeta potentials of the Au@GSH NPs and their functionalized products range from −33.7 to −22.1 mV. (c) Qualitative assessment of the peptide presence on the NPs' surface by agarose gel electrophoresis. The microcentrifuge tubes (top) show the sample preparations before electrophoresis. Differences in the mobility of the NPs after conjugation with peptide and drug were observed due to their difference in charge. NPs with surface peptide give a smear on the gel image (bottom). An equal volume of conjugated sample was loaded in all the lanes. Sample concentrations were 1 mg/mL except Au@GSH NPs, which were used at 2 mg/mL to aid identification.

free peptide, and functionalized nanocarriers (Au@CRGDK, Au@Pt(IV), and Au@Pt(IV)+CRGDK) were evaluated against two different prostate cancer cells (PC-3 and DU-145) using MTT assays and flow cytometry studies (Figure 3). These two cell lines were selected because PC-3 cells overexpress the Nrp-1 receptor (indicated as Nrp-1 positive), while DU-145 cells have low levels of Nrp-1 expression (indicated as Nrp-1 negative).

In our studies, no cytotoxicity was observed when both cell lines were treated with free peptide (100 μg/mL/0.00018 mM) (data not shown) and Au@GSH NPs (100 nM), even after 72 h of incubation (Figure S6, Supporting Information). This suggests that GSH-stabilized small NPs show good biocompatibility, in accord with previously reported values.[33] However, after the functionalization of the NPs with peptide, a slight decrease in cell viability was observed after 72 h of incubation, which might be due to higher uptake (Figure S6, Supporting Information).[10]

Increased cytotoxicity was observed after the treatment of cells with nanocarriers that were functionalized with drug and targeting peptide (Au@Pt(IV)+CRGDK). The IC_{50} value for Au@Pt(IV)+CRGDK was found to be 1.6 μM. The Au@Pt(IV)+CRGDK NPs were 28.13-fold more cytotoxic than platinum(IV), 8.25-fold more cytotoxic than Au@Pt(IV) NPs, and 2.62-fold more cytotoxic than cisplatin (Figure 3a and b). This higher efficacy was most likely due to increased delivery of drug molecules into cancer cells. Therefore, Au@Pt(IV)+CRGDK was selected as the most effective candidate among the four nanocarriers.

When Au@Pt(IV)+CRGDK was used to treat DU-145 (Nrp-1 negative) cells, the IC_{50} value was 2.5-fold lower than for PC-3 (Nrp-1 positive) cells (Table S1 and Figure S7, Supporting Information).

One explanation why Au@Pt(IV)+CRGDK NPs are more cytotoxic than cisplatin is that NPs can adsorb onto the cell membrane, creating a concentration gradient that favors drug influx into prostate cancer cells. Another explanation is that tumor cells, which frequently show enhanced levels of endocytosis, can directly internalize the NPs, thus allowing intracellular drug release. Our finding that Au@Pt(IV)+CRGDK was more effective in Nrp-1 positive cells (PC-3) that in

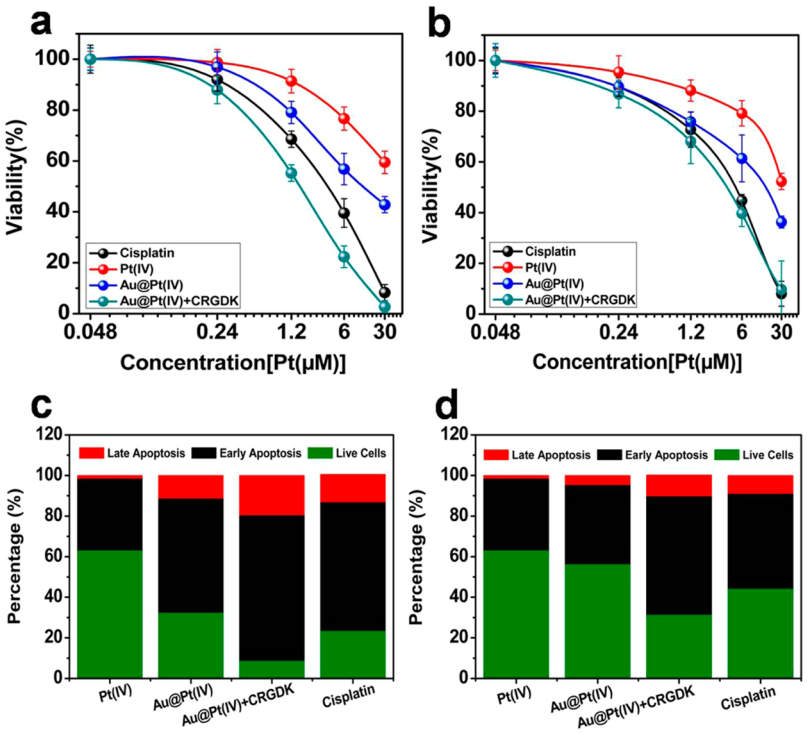

Figure 3. Cytotoxicity effects of cisplatin, platinum(IV), Au@Pt(IV) NPs, and Au@Pt(IV)+CRGDK NPs measured by MTT assays and flow cytometry. Viability of cells was determined using MTT assays after 72 h treatment with drugs or functionalized nanocarriers (dosage 0.048−30 μM) in PC-3 (a) and DU-145 (b) cells. Flow cytometry assays to detect apoptotic effects in PC-3 (c) and DU-145 (d) cells after treatment with the same drugs and NPs (5 μM) for 24 h. Au@Pt(IV)+CRGDK NPs caused the greatest decrease in cell viability and induced the highest levels of apoptosis. A stronger effect was observed in PC-3 (Nrp-1 positive) cells than DU-145 (Nrp-1 negative) cells.

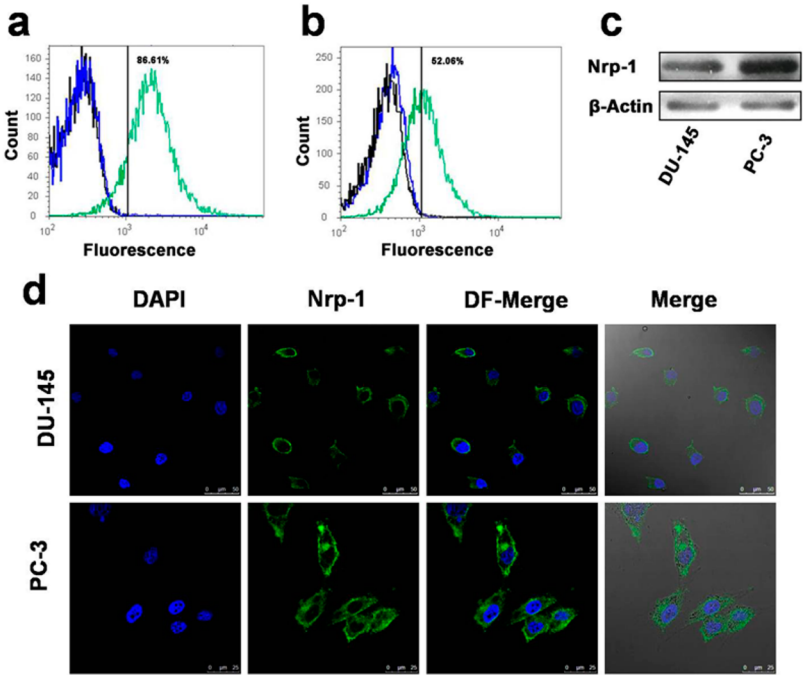

Figure 4. Level of Nrp-1 receptor expression in PC-3 and DU-145 prostate cancer cells: Nrp-1 expression in PC-3 (a) and DU-145 (b) detected by flow cytometry. Here the cells treated only with secondary antibody were kept as a negative control. (c) Nrp-1 protein expression analysis in PC-3 and DU-145 cells through Western blotting. (d) Expression of Nrp-1 was detected with FITC-labeled anti-Nrp-1 antibody (green) on the membranes of PC-3 and DU-145 cells through confocal microscopy. Nuclei of the cells are stained with DAPI (blue) (scale bars, 50 μm for DU-145 and 25 μm for PC-3). "DF-Merge" shows merged DAPI and FITC images. "Merge" shows merged DAPI, FITC, and bright field images.

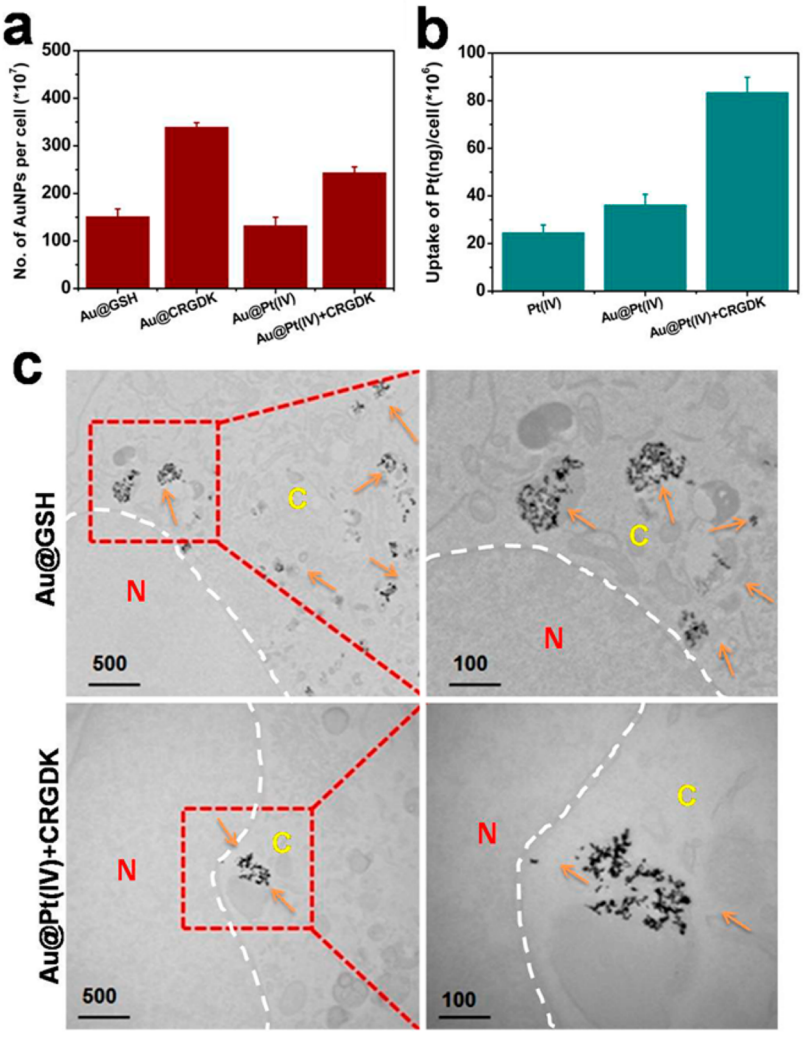

Figure 5. Uptake efficiency of NPs and platinum drug: (a) Cellular uptake of NPs after 72 h treatment with Au@GSH, Au@CRGDK, Au@Pt(IV), and Au@Pt(IV)+CRGDK NPs. (b) Determination of the platinum (Pt) concentration in cells after incubation with Pt(IV), Au@Pt(IV), and Au@Pt(IV)+CRGDK for 72 h. (c) TEM images of prostate cancer cells (PC-3): Cells were incubated with drug and peptide-functionalized nanocarriers (Au@Pt(IV)+CRGDK dose (100 nM) equivalent with the cytotoxicity assay). The images indicate the endocytosis and intracellular uptake of NPs into prostate cancer (PC-3) cells. Most of the NPs are well distributed in the cell cytoplasm and localized near the nuclear membrane. Bars represent 500 nm (left) and 100 nm (right), and arrows highlight internalized gold nanoparticle aggregates in endosomes/lysosomes. "N" represents the nucleus and "C" represents the cytoplasmic region.

Nrp-1 negative cells (DU-145) suggested that receptor-mediated endocytosis, triggered by binding of CRGDK to Nrp-1, might play a significant role in enhancing the cytotoxicity of Au@Pt(IV)+CRGDK.

We further analyzed the effects and target specificity of the functionalized nanocarriers compared to free drug (platinum(IV) and cisplatin) using a flow cytometry assay to detect apoptotic cells (Figure 3c and d). A lower dose (5 μM) was used to treat the cells for the first 24 h to check the specificity of the nanocarriers. The results were in accordance with expectations: more apoptotic cells were detected in PC-3, which overexpresses Nrp-1, than in DU-145, which expresses low levels of Nrp-1. This result indicates the target specificity of the functionalized peptide.

Receptor Expression and Function. To further confirm the role of Nrp-1 in cellular uptake and cytotoxicity, we evaluated the level of Nrp-1 protein expression in both cell lines *via* flow cytometry (Figure 4a), Western blotting analysis (Figure 4b), and confocal microscopy (Figure 4c). Data obtained from these techniques suggested that Nrp-1 expression is higher (86.61%) in PC-3 cells than in DU-145 cells (52.06%).

Cellular Uptake and Localization Study. Various factors are known to affect the difference in cellular uptake of NPs such as size and shape of the nanomaterials,[42] rate of physiochemical processes,[43] different functionality, properties of the protein corona,[44] and cellular environment.[45] However, there is a lack of consensus regarding the uptake of NPs with different functionalities and how this plays a role in the transport of the

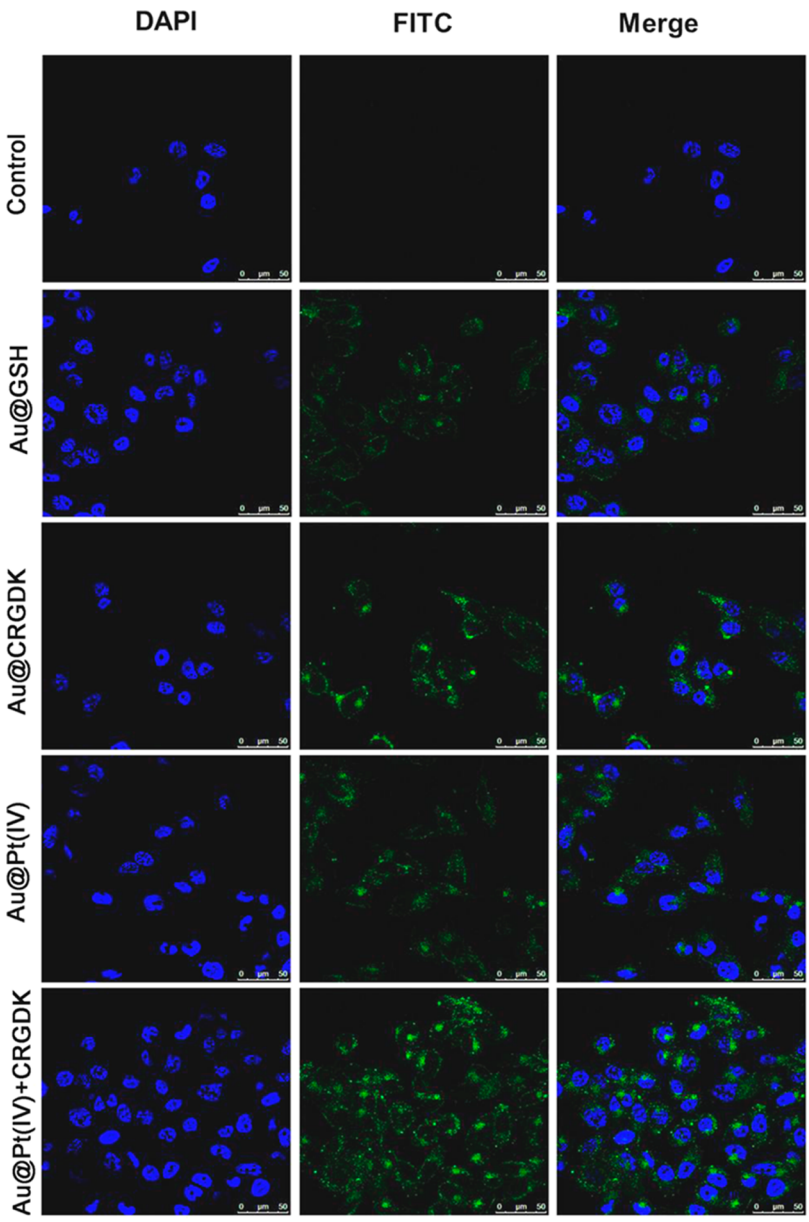

Figure 6. Localization study of Au@GSH NPs: Confocal images of prostate cancer (PC-3) cells incubated with FITC-conjugated functionalized nanocarriers (green signal) at a dose equivalent with the cytotoxicity assay. Nuclei of the cells were stained with DAPI (blue). In target-functionalized nanocarriers, differential fluorescence activity was observed as compared with nanocarriers that did not carry the targeting peptide. Individual interference contrast transmission images were obtained and then overlaid in maximal projection mode. Scale bars represent 50 μm.

pharmaceutical agents they carry. In our study we have attempted to investigate whether the functionalization of nanocarriers with a therapeutic drug and a targeting peptide influences the overall cellular localization or uptake by the cancer cells.

We next used ICP-MS to determine the uptake efficiency of gold NPs[33] and platinum(IV) drug[40] in cells treated with different functionalized nanocarriers. The final concentration of NPs and drug was determined by calculating the Au and Pt atom concentrations in different functionalized nanocarriers. When the nanocarriers were compared, significant differences in cellular uptake were observed (Figure 5a).

High levels of uptake were found for Au@CRGDK and Au@Pt(IV)+CRGDK, whereas low uptake levels were observed for Au@Pt(IV) and Au@GSH because of the absence of the targeting peptide (CRGDK). Similarly, in cells treated with Pt(IV), Au@Pt(IV), and Au@Pt(IV)+CRGDK (Figure 5b), the intracellular (Pt) level was highest when the targeting peptide was present on the NP's surface. Thus, the experimental results support our hypothesis that the presence of ligands strongly influences the uptake of NPs by cancer cells.[46]

We expected that the small Au@GSH NPs (5.2 nm) might have the capability to penetrate the nucleus of

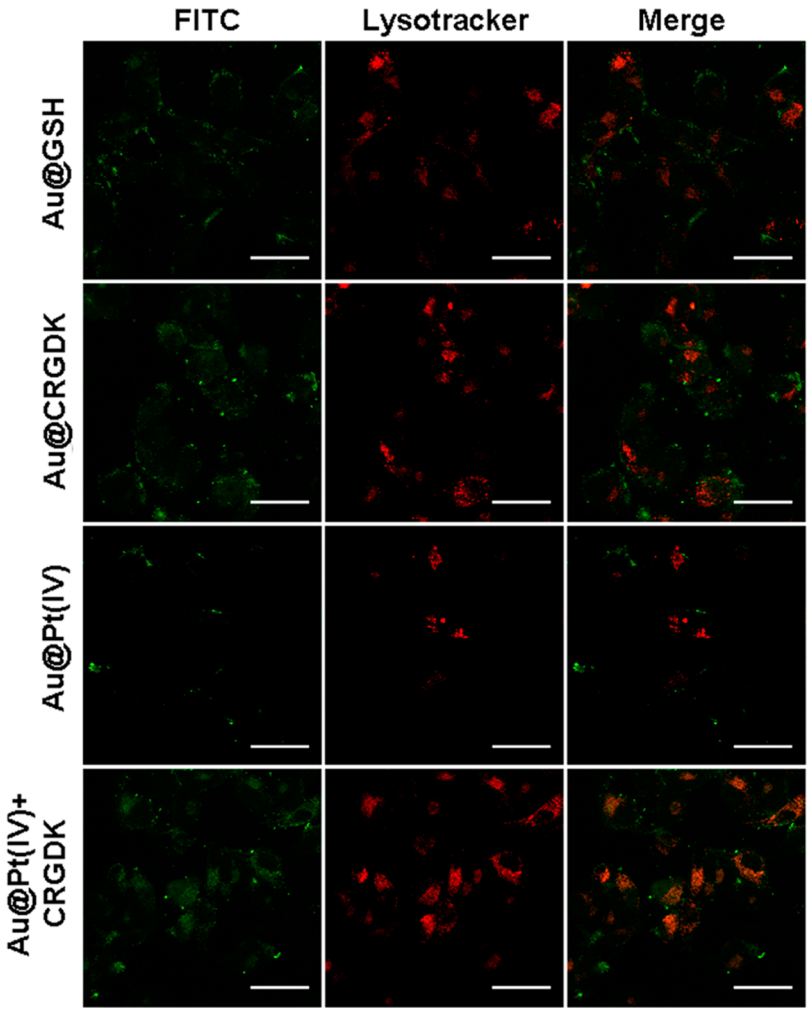

Figure 7. Subcellular localization study of Au@GSH NPs: Prostate cancer (PC-3) cells were cultured with different functionalized nanocarriers (100 nM) for 4 h at 37 °C in 35 mm glass microscopy dishes. Cells were imaged using a Zeiss confocal microscope. Lysotracker red (DND-99) was used to stain endosomes and lysosomes. Scale bars represent 50 μm.

cancer cells. In our previous study, we observed that 2 and 6 nm gold NPs stabilized with tiopronin (Au@tiopronin) are localized in both the cytoplasm and the nucleus.[32] However, in this study we were unable to observe the localization of glutathione-stabilized NPs (Au@GSH) in the nuclear compartment of the cells, which might be because the GSH molecules on the surface of the NPs have different effects than tiopronin on the pathways for nuclear internalization.[47,48]

During this study, we observed that the NPs were well distributed in the cytoplasm and also localized in close proximity to the cell nucleus of PC-3 cells (Figure 5c). Nanoparticles was observed within subcellular compartments such as endosomes or lysosomes (Figure 5c), confirming that the NPs had been taken up by acidic organelles. The drug would then be released from the acidic compartments and affect the viability of the cancer cells.

Internalization and Distribution of Targeted Functionalized Nanocarriers. Cells also have unique properties, collectively termed the "cell selective response", and this phenomenon always varies from cell to cell with the different physiochemical properties of the nanomaterials.[45] Some reports suggest that the cellular uptake and localization of NPs in normal and cancer cells vary according to the size, the condition of the cells, and the methodology applied to enhance their uptake efficiency (*e.g.*, radiation and sources of external stimuli).[48]

To confirm this hypothesis, we functionalized the same nanocarriers with a fluorescent molecule (FITC) (Figure S8) and then examined their intracellular distribution using confocal microscopy. Both the prostate cancer cells (PC-3 and DU-145) were incubated with 100 nM of different functionalized nanocarriers for 4 h before detecting the fluorescence signal (green). We found that the fluorescence intensity was high for targeted NPs (carrying the CRGDK peptide) when compared to nontargeted NPs (Figure 6) in both cell lines.

However, the same functionalized nanocarriers displayed lower fluorescence intensity (Figure S9) in

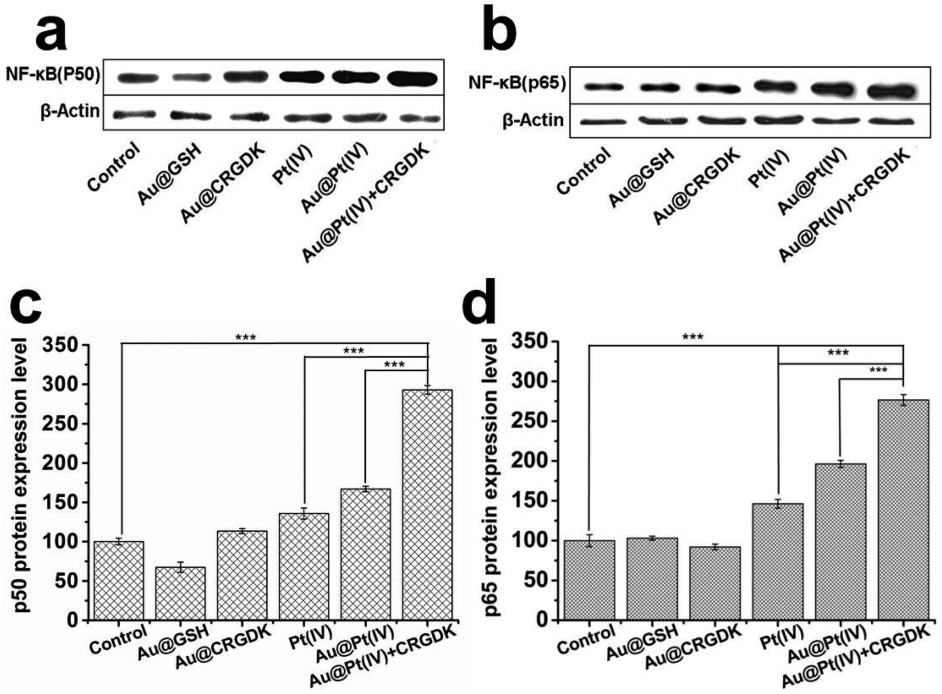

Figure 8. Intracellular mechanism of platinum(IV) drug activity and NF-κB protein expression profile: Expression of NF-κB proteins (p50 and p65) in PC-3 cells measured by Western blot analysis (a, b) and comparison of protein expression levels (c, d) following different treatments. After treatment of the cells with Pt(IV), Au@GSH NPs, and functionalized nanocarriers, total protein (20 μg/mL) was separated on a gel (10%), transferred to a PVDF membrane, treated with primary antibodies against p50 or p65, washed, and then treated with peroxidase-conjugated secondary antibody.

DU-145 cells than in PC-3 cells due to low expression of Nrp-1 receptor in DU-145 cells. This result proves that the amount of NP uptake into the cell cytoplasm is dependent upon the level of Nrp-1 cell surface receptor. The fluorescence signal was higher for targeted NPs (Au@CRGDK) than for nontargeted NPs (Au@GSH and Au@Pt(IV)) in both Nrp-1 positive (PC-3) and Nrp-1 negative (DU-145) cells, thus demonstrating that CRGDK enhanced the targeting efficacy.

The subcellular internalization of Au@GSH NPs and their functionalized derivatives was examined after 4 h treatment by confocal laser scanning microscopy. Lysotracker red (DND-99) was used to track gold NPs into the endosome/lysosome compartment. In cells treated with target-functionalized nanocarriers, most of the nanocarriers were localized in the lysosomes and cytoplasm (Figure 7). The difference in fluorescence signal between the treatments can be explained by the targeting specificity. Due to pH sensitivity of endosomes (pH 5.0−6.0) or lysosomes (pH 4.0−5.0), the target-functionalized nanocarriers easily disintegrate and get distributed in the cell cytoplasm.

Competition Assay. We carried out a competition assay to determine whether the target-functionalized nanocarriers specifically interacted with Nrp-1 in PC-3 cells. The cells were pretreated with excess anti-Nrp-1 monoclonal antibody and incubated with Au@CRGDK and Au@Pt(IV)+CRGDK (100 nM). The antibody-treated cells showed much lower levels of nanocarrier uptake than untreated cells (Figure S10), supporting our hypothesis that the CRGDK-modified nanocarriers interact specifically with neuropilin-1 receptors.

Mechanism of Platinum(IV) Drug Activity in Cancer Cells. Cisplatin, which has been used to treat prostate cancer, is a DNA-damaging agent that induces apoptosis. Some studies suggest that cisplatin induces the activation of NF-κB, resulting in increased cisplatin resistance.[50] NF-κB activation can protect cells from apoptosis by enhancing the expression genes encoding several survival factors, such as the Bcl-2 homologues Bfl-1 and Bcl-Xl and members of the inhibitors of apoptosis family.[51]

NF-κB upregulates the expression of many genes, including those encoding death receptor 4 (DR4, DR5), TNF-related apoptosis-inducing ligand (TRAIL), Fas, and Fas ligand, which are implicated in promoting apoptosis. Several "death genes" have potential NF-κB binding sites in their promoters. Thus, many lines of evidence suggest that exogenous signals such as platinum-based drugs and reactive oxygen species induce apoptosis by a NF-κB-based mechanism.[51]

Activation of NF-κB (which requires phosphorylation and ubiquitin-mediated degradation of IκBα by the IKK complex) plays an essential role in platinum-induced apoptosis in human cancer cells.[52,53]

Therefore, to confirm the intracellular mechanism of platinum(IV), we analyzed the (NF-κB) protein (p50 and p65) expression in the PC-3 cell line through Western blotting. Electrophoretic mobility shift assays (EMSAs) were performed with an NF-κB-specific

binding site probe using nuclear extracts collected from control cells and from cells treated with platinum(IV) drug or targeted nanocarriers (Au@Pt(IV)+CRGDK). Increased levels of DNA−protein complexes were observed in extracts from PC-3 cells treated with free drug or Au@Pt-(IV)+CRGDK compared to negative controls or untreated cells (Figure S11). A higher level of NF-κB activation was detected in cells treated with Au@Pt(IV)+CRGDK compared to free drug. These results can be evaluated by comparing them to positive control cells, which were treated with the NF-κB activator TNF-α (Figure S11). Taken together, the above results indicate an increase in NF-κB activity in platinum-treated prostate cancer cells.

During these studies, we observed high levels of p50 and p65 protein expression in cells treated with target-functionalized nanocarriers (Au@Pt(IV)+CRGDK) compared to controls (Au@GSH NPs and free drug) because of the presence of CRGDK, which results in enhanced delivery of platinum(IV) into the cancer cells (Figure 8). Au@Pt(IV), which lacks the targeting peptide, showed lower cytotoxicity and lower levels of p50 and p65 protein expression than Au@Pt(IV)+CRGDK (Figure 8). Importantly, our results strongly suggest that the nanocarriers may mediate cancer cell apoptosis by interacting with the NF-κB pathway. In addition, our nanocarriers have the ability to target specific cells and successfully deliver drugs into cancer cells.

CONCLUSION

In this study, we have developed a targeted drug delivery strategy based on GSH-stabilized gold NPs for platinum-based anticancer drugs. We designed a basic and effective gold NP nanocarrier (Au@Pt(IV)+CRGDK) consisting of a platinum(IV) drug as well as a receptor-targeting peptide, and we studied the bioeffects of functionalized nanocarriers on prostate cancer cells. The cytotoxicity and uptake efficiency of the target-functionalized nanocarrier (Au@Pt(IV)+CRGDK) is superior to that of nontargeted systems (Au@GSH, Au@Pt(IV)). In the Nrp-1 negative cell line (DU-145), no obvious enhancement was observed compared to the Nrp-1 positive cell line (PC-3). Our results indicate that when the NPs attach to the cell surface, the CRGDK peptide successfully targets the Nrp-1 receptor, which binds to the CendR motif, resulting in greater cell penetration and internalization efficiency. Functionalized gold NPs, such as Au@Pt(IV)+CRGDK, could significantly increase the intracellular uptake and cytotoxicity of NPs and drug and at the same time interact with NF-κB to trigger platinum-induced apoptosis in prostate cancer cells. Compared to PC-3 cells, DU-145 cells show a relatively minor enhancement of NPs and drug uptake. Therefore, CRGDK-modified nanocarriers may have great potential for targeting cancer cells, and such a system may further be used to target metastatic cancers, which occur during the advanced stages of disease.

However, the application of therapies based on platinum drugs is limited due to serious side effects that are intrinsic or acquired through development of resistance. Therefore, basic research and new methods are essential for further development of novel platinum-based therapeutic drugs. In the future, we would like to design an environmentally responsive system that combines the platinum(IV) drug with a targeted drug delivery system to control drug release, thereby reducing toxicity to normal tissues and enhancing the antitumor effect. In summary, by functionalizing gold nanoparticles with a platinum(IV) drug and a targeting peptide, we have developed a novel approach to cancer therapy that holds significant promise for cancer treatment in the future.

EXPERIMENTAL SECTION

Chemicals and Reagents. Gold(III) chloride trihydrate (99.9%), sodium borohydride ($NaBH_4$; >98.0%), (*N*-(3-(dimethylamino)-propyl)-*N*-ethylcarbodiimidehydrochloride (EDC), sodium (98%), *N*-hydroxysuccinimide (NHS; >97%), cisplatin (*cis*-$[Pt(NH_3)_2(Cl)_2]$; ≥99.9%), and succinic anhydride ($C_4H_4O_3$; ≥99%) were purchased from Sigma-Aldrich (St. Louis, MO, USA). Glutathione (GSH) ($C_{10}H_{17}N_3O_6S$; >98%) and anhydrous dimethylformamide (DMF) were purchased from Alfa Aesar. Hydrogen peroxide (H_2O_2) was purchased from Beijing Donghualituo Technology Development Co., Ltd. Nitric acid, HCl, ether, acetone, and isopropyl alcohol were obtained from Beijing Chemical Reagents Institute (China). Standard solutions of gold and platinum (1000 μg/mL) were obtained from the National Analysis Center for Iron and Steel, China. All chemicals and reagents were used without further purification, and Milli-Q (18.2 MΩ·cm) water was used throughout this study. All glassware employed for the synthesis of the nanoparticles, drug synthesis, and storage was completely cleaned with aqua regia (HCl:HNO_3 = 3:1).

Cell culture media (RPMI-1640) and reagents were purchased from Media Tech. Cell proliferation kit and 3-(4,5-dimethylthiazolyl-2)-2,5-diphenyltetrazolium bromide (MTT) were purchased from Promega Corporation (USA), while peptide (CRGDK) was obtained from GL Biochem (Shanghai, China). Antibody Nrp-1 (neuropilin-1) (ab81321 rabbit-mAb) and p50 antibody (ab7971, rabbit-pAb) were purchased from Abcam (BioSci & Tech. Ltd. Co, Beijing China), anti-p65 (BS3157, rabbit-pAb) was obtained from Bioworld Technology, Inc., USA, antibody anti-β-actin (sc47778 mouse mAb) was obtained from Cell Signaling (Shanghai, China), goat-anti-mouse IgG (ZB-2305) was obtained from Z.G.B. Biotec. Co. Ltd. (Beijing, China), and goat-anti-rabbit IgG (cat no. 31460) was from Thermo Scientific (Rockford, IL, USA). NF-κB antibody and protein marker (P7708S) were from New England Bio-Laboratories. The sequence of double-stranded oligonucleotides (5′-AGTTGAGGGGACTTTCC-CAGGC-3′) containing a consensus binding site for c-Rel was obtained from Santa Cruz Biotechnology. Buffers were prepared according to standard laboratory procedures and were sterilized and filtered through 0.22 mm membranes (Whatman Inc., Sanford, ME, USA) for further biological experiments.

Instrument Measurements. TEM (Tecan-G2-20-S, TWIN, FEI, Hillsboro, OR, USA) was used for NP size measurement. UV−vis spectra were obtained using a Lambda-950-PE spectrophotometer (PerkinElmer, Waltham, MA, USA). Surface charge distribution was studied by determining the zeta potential (Zetasizer-MALVERN, Worcestershire, UK). Confocal microscopy

experiments were performed with an LSM 710 (Carl Zeiss AG, Oberkochen, Germany), localization studies of Au@GSH NPs were performed through a Bio-TEM (Hitachi HT7700, 120 kV, Biomedical TEM), and ESI-MS mass spectra were recorded on a Bruker Amazon ES ion trap spectrometer (Bruker Co., Bremen, Germany). Fourier transform infrared spectroscopy was conducted with a Spectrum One (PerkinElmer, Waltham, MA, USA), NMR spectra were analyzed by using AVANCE III 400 (Bruker Co., Bremen, Germany), and X-ray photoelectron spectroscopy was performed with an X-ray photoelectron spectrometer (ESCALAB 250Xi, Thermo Scientific, Waltham, MA, USA). Cell cytotoxicity assays were measured with a plate reader (TECAN Infinite-M200, Männedorf, Switzerland) and by flow cytometry using an Attune acoustic focusing cytometer (Applied Biosystems, Life Technologies, Carlsbad, CA, USA). The concentration of gold and platinum was calculated *via* ICP-MS (ELANDRC-PerkinElmer, Waltham, MA, USA).

Synthesis of Glutathione-Stabilized Gold Nanoparticles. The process for the synthesis of GSH-stabilized gold NPs is shown in Scheme S1 and described in detail in the Supporting Information.

Synthesis of the Platinum(IV) Drug. The process for the synthesis of the platinum(IV) complex began with the parent complex, cisplatin. In the initial step, cisplatin was oxidized with H_2O_2 to form complex **1**, bearing two hydroxyl groups at its axial positions, as shown in Scheme 2. In further steps these hydroxyl groups were reacted with succinic anhydride to afford complex **2** with a good yield of 85%. Further details of the steps involved in the synthesis, purification, and characterization of platinum-(IV) can be found in the Supporting Information.

Functionalization of Au@GSH NPs with Targeting Peptide (CRGDK) and Platinum(IV) Drug. The details of the process by which Au@GSH NPs were functionalized with CRGDK peptide and platinum(IV) drug are described in the Supporting Information.

Quantification of Peptide and Drug Conjugation on the Surface of Au@GSH NPs. To quantify the amount of peptide loaded onto the surface of NPs, we adopted the BCA method. Unconjugated NPs were diluted (160 μg/mL) and kept as a blank (negative control). Free peptide at a concentration of 160 μg/mL was kept as a positive control. Concentrations of NPs in the conjugated samples (Au@CRGDK and Au@Pt(IV)+CRGDK) were similar to that of the blank, and the exact concentration of peptide on both the nanocarriers was determined through the BCA assay. The values for optical density (OD) at 570 nm were plotted on a standardized curve, and the amounts of peptide in the conjugated samples were calculated using the following formula (eq 1). The OD values were not affected by Au@GSH NPs during this assay.

$$\begin{aligned}\textbf{Amount of surface peptide} &= [\mathrm{OD}_{570}\text{ of Au@peptide} \\ &\quad - \mathrm{OD}_{570}\text{ of background})] - [\mathrm{OD}_{570}\text{ of control} \\ &\quad - \mathrm{OD}_{570}\text{ of background})] \\ \textbf{Amount of peptide} &= \text{Au@peptide} - \text{Au@GSH} \\ Y &= A + BX\ \text{[from standard graph]} \\ X &= (Y - A)/B \end{aligned} \quad (1)$$

where Y = actual OD_{570} of the sample, A = constant, and B = coefficient; the values for both A and B were obtained from linear fitting; $X = \mu$g/mL was calculated by substituting the value of A and B in the above equation.

To determine the amount of platinum(IV) drug loaded onto the nanocarriers, Pt quantification was performed using ICP-MS. Instruments were optimized in order to obtain maximum sensitivity for Pt atoms. The most abundant isotopes of Pt were used as an internal standard and measured at m/z 195. A blank and three standards were used for calibration, after which platinum-containing nanocarriers (fully dried) were further dissolved in 5 mL of 2% HNO_3. The solution was treated in an ultrasonic bath for several minutes, and a clear solution was obtained for assessment of total Pt concentration. All measurements were performed in triplicate, and the amount of Pt loaded onto the surface of each nanocarrier was calculated using the following equation (eq 2).

$$\text{Loading efficiency (LE\%)} = \frac{[\mathrm{Pt}]^{\mathrm{i}} - [\mathrm{Pt}]^{\mathrm{f}}}{[\mathrm{Pt}]^{\mathrm{i}}} \times 100\% \quad (2)$$

where $[Pt]^i$ is the initial and $[Pt]^f$ is the final concentration of Pt in the measuring solution.

Cell Culture and Cytotoxicity Assay. Human prostate adenocarcinoma cells PC-3 and DU-145 were obtained from Peking Union Medical College, Beijing, China. Cells were grown in RPMI-1640 medium containing 10% fetal calf serum, 2 mM L-glutamine, penicillin (100 U/mL), and streptomycin (100 μg/mL). Both cell lines were maintained at 37 °C in the presence of 5% atmospheric CO_2.

Treatment of Cells with Au@GSH NPs and Functionalized Nanocarriers. Cells (PC-3 and DU-145) were seeded in 96-well plates at a density of 3×10^4 cells/well/100 μL, incubated for 24 h, and then treated with free peptide (CRGDK, 100 μg/mL), Au@GSH NPs (60 μM), peptide-conjugated NPs (Au@CRGDK), cisplatin, platinum-(IV) drug (complex **2**), and drug-conjugated NPs (Au@Pt(IV) and Au@Pt(IV)+CRGDK) at a final equivalent platinum concentration of 30 μM for the last four samples. Equivalent concentrations of Au were maintained for all nanocarrier systems.

Cells were further incubated for 72 h, following which cell viability was determined using the MTT assay. Briefly, 100 μL of MTT solution (0.5 mg/mL) was added to each well following treatment and incubated for 4 h at 37 °C, and then MTT solution was replaced with 100 mL of DMSO (dimethyl sulfoxide). The plates were read at 570 nm in a microplate reader (TECAN-Infinite-M200). Viability of control cells (untreated) was kept at 100%. Viable cell percentage was calculated using the following equation (eq 3), and IC_{50} values were determined by interpolation of the resulting curves.

$$\text{Cell lethality (\%)} = \frac{1 - (\mathrm{OD}_{570}\text{ of sample} - \mathrm{OD}_{570}\text{ of blank sample})}{\mathrm{OD}_{570}\text{ of control} - \mathrm{OD}_{570}\text{ of blank}} \times 100\% \quad (3)$$

where "sample" refers to treated cells and "control" refers to untreated cells.

Measurement of Apoptosis. Both the cell lines were grown in six-well plates (2×10^5 cells/well) overnight at 37 °C. The medium was replaced with fresh RPMI-1640 after 24 h along with cisplatin, platinum(IV), and drug-conjugated Au@GSH NPs (Au@Pt(IV) and Au@Pt(IV)+CRGDK), individually with similar concentrations of Pt in all sample. After the incubation period, cells were washed with ice-cold PBS, harvested through trypsin, and centrifuged at 1000 rpm for 5 min. The cells were counted, and each sample was again suspended in 100 μL of binding buffer, 5 μL of R-PE annexin V, and 1 μL of SYTOX (1 μM) and incubated for 15 min. Then 500 μL of binding buffer was added, and the samples were kept on ice until analysis through flow cytometry. Emission of fluorescence was measured at 530 and 575 nm and using a 488 nm excitation wavelength. Apoptosis was evaluated using an FITC annexin V and propidium iodide (PI) kit for flow cytometry (Invitrogen, Molecular Probes). Cells that were negative for both PI and annexin V staining were considered to be live cells, while the cells that were PI-negative and annexin V-positive were considered to be early apoptotic cells. Cells that showed both PI-positive and annexin V-positive staining are those in the later stages of apoptosis and are considered as dead cells.

Flow Cytometry and Confocal Microscopy Studies of Protein Expression. Cells treated with drug and nanocarriers were harvested from six-well plates by treatment with trypsin, counted, and washed with ice-cold PBS. A total of 5×10^5 cells were incubated with fixing solution (4% paraformaldehyde) for 15 min at room temperature after washing with ice-cold PBS. Blocking was conducted by incubation with 10% goat serum (PBS diluted) for 1 h at 25 °C. After washing steps, cells were incubated with primary Nrp-1 antibody (rabbit mAb) (1:50) overnight at 4 °C, then washed again and incubated with FITC-conjugated secondary (goat anti-rabbit) (1:500) for 1−1.5 h. After the incubation period again cells were washed three times with 0.5 mL of ice-cold PBS and resuspended in 500 μL of the same mixture. Flow cytometry analysis was performed, and the fluorescence intensity was collected to confirm Nrp-1 expression.

For confocal microscopy a total of 5×10^4 cells per well were incubated with primary antibody (rabbit mAb, 1:50) and secondary antibody (goat anti-rabbit IgG conjugated with FITC, 1:500 dilution). The plate was introduced into the confocal

microscopy chamber, and the laser was excited at wavelengths of 405 nm (DAPI) and 488 nm (FITC).

Quantification of Cellular Uptake of Au@GSH NPs. For the study of cellular uptake of NPs and drug, cells were grown in two six-well culture plates: one for the detection of Au atoms and another for the detection of Pt atoms. Around 5×10^5 cells per well were grow to 80% confluence. The cells were then treated with 100 nM Au@GSH NP or its conjugated derivatives, similar to the MTT assay, and incubated for 72 h. To remove excess or unbound NPs from the outer cells, the surface was thoroughly washed two or three times with PBS (1×) and then digested in aqua regia (HCl/HNO_3) with a v/v ratio of 3:1. Analysis of the results was performed using ICP-MS, and the amount of gold NPs was calculated based on the atom concentration of Au and the Pt found in the samples compared to standard Au and Pt solutions.

TEM Sample Preparation for Localization Study of Au@GSH NPs. For TEM analysis, the cells were harvested after trypsin treatment, suspended in PBS, and fixed with solution containing 2.5% (v/v) EM-grade glutaraldehyde in PBS at pH 7.4 for 12−16 h. After the fixation process, the cells were gently pelleted and washed in H_2O and then dispersed into Noble agar worms and stained (or not stained) with 2% osmium tetroxide and 2% uranyl acetate. Before embedding into Eponate 12 resin, cells were completely dehydrated in ethanol and acetone, and then sample resin blocks were trimmed and sectioned (50−60 nm) on an MT-X Ultra microtome using a 45 diatom diamond knife. An ultrathin section were cut and placed on 200 mesh copper grids coated with Formvar/carbon for observation under the transmission electron microscope (H-7650B) at 30 kV and a working distance of 6.7 mm.

Intracellular Localization Study of Nanocarriers by Confocal Microscopy. For visual assessment of cellular uptake of NPs, cells were seeded in confocal disc chambered cover glasses (Corning Ltd.) at a density of 1.0×10^5 cells/well in 500 μL of RPMI-1640-containing medium. After 24 h of incubation a solution of FITC-functionalized nanocarriers (Figure S8) was added to each well at a concentration similar to the cytotoxicity assay, followed by 4 h of incubation at 37 °C. The cells were then washed three times with PBS (pH 7.4) under gentle shaking and later fixed in 4% paraformaldehyde solution. Finally, the cells were washed three times with PBS, and nuclei of the cells were stained with DAPI for 1−2 min. Observations were made with a confocal laser scanning microscope using excitation wavelengths of 405 nm (DAPI) and 488 nm (FITC).

Evaluation of Lysosomal Acidity. A total of 5×10^4 cells per well were incubated with Au@GSH NPs and functionalized derivatives for 4 h; then the cells were washed two or three times with PBS. After that, the cells were incubated in a humidified incubator for 30 min at 37 °C in 5% CO_2 under growth conditions with 500 μL of prewarmed medium containing 5 μmol/L Lysotracker red (DND-99) dye. Cells were examined by confocal laser scanning microscopy using excitation wavelengths of 405 nm (DAPI), 488 nm (FITC), and 570 nm (Lysotracker red).

Competition Assay. PC-3 cells seeded in 35 mm glass microscopy dishes were grown overnight in complete medium. Cells were incubated for 30 min in serum-free medium, blocked with 5% BSA (diluted with serum-free medium) for 30 min at 37 °C, and then treated with excess anti-Nrp-1 primary antibody (1:50, Ab81321; Abcam, Cambridge, MA, USA) in serum-free medium for 15 min. The cells were washed with PBS, incubated with Au@GSH NPs and functionalized derivatives (concentration equivalent to the MTT assay) for 1 h at 37 °C, and then fixed in solution containing 4% cold paraformaldehyde for 20 min. Nuclei were stained with DAPI (20 μg/mL) for 5 min. The cell−surface distribution of the NPs was observed using a confocal microscope.

Analysis of NF-κB Protein Expression. Cells treated with Pt(IV), Au@GSH NPs, and functionalized derivatives were washed two or three times with ice-cold PBS (1×) and resuspended in cold lysis buffer containing 0.5 mM PMSF. Cells lysates were centrifuged for 15 min at 13000*g*, and the total protein concentration of the supernatant was determined by spectrophotometer. A total of 16 μg of protein in 20 μL was loaded onto a sodium dodecyl sulfate-polyacrylamide gel (SDS-PAGE). A gel (10%) was used for the detection of NF-κB protein, whereas a gel (8%) was used for detection of Nrp-1 protein. Gels were blotted onto 0.2 mm PVDF membranes, which were incubated in 5% milk (skimmed) in TBST containing 0.1% Tween 20 for 24 h at 4 °C. Membranes were incubated with anti-p50 or anti-p65 primary rabbit polyclonal antibodies (pAb) at 1:1000 dilutions for 3 h at room temperature (for p50) or at 4 °C overnight (for p65) in TBS with 2% milk and goat anti-mouse IgG secondary antibody (1:5000 (v/v)) conjugated with peroxidase, for 2 h at room temperature in TBS buffer. Nrp-1 was detected with a rabbit monoclonal antibody (mAb) (diluted 1/1000 v/v) as the primary antibody and peroxidase-conjugated goat anti-rabbit (diluted 1:5000 v/v) as the secondary antibody. Membranes were also treated with a mouse monoclonal β-actin antibody (diluted 1:200 v/v) and peroxidase-conjugated IgG (diluted 1:5000 v/v) goat anti-mouse as an internal standard. Finally, Kodak X-Omat film was used with ECL reagent for membrane development, and intensities of the individual protein bands were determined by densitometry.

Electrophoretic Mobility Shift Assays. The nuclear extract process was carried out using the manufacturer's instructions (Applygen Technologies Inc., Beijing, China). Oligonucleotides sequences (5′-AGTTGAGGGGACTTTCCCAGGC-3′) that contain a consensus binding site for c-Rel were labeled using biotin at the 5′-end. Approximately 3 μg of nuclear extracts was incubated with labeled oligonucleotide (1 μL) in 15 μL of incubation buffer containing Tris-HCl (10 mM), NaCl (40 mM), EDTA (1 mM), beta-mercaptoethanol (1 mM), and glycerol (2%) in buffer solution for more than 20 min at 25 °C. The specificity of NF-κB protein and binding activity of DNA was confirmed by competition with mutant or cold (non-biotin-labeled) oligonucleotide. The complexes (DNA−protein) were resolved by electrophoresis in nondenaturing polyacrylamide gels (7%) and analyzed by autoradiography.

Statistical Analysis. Each experiment was composed of three parallel samples, and standard statistical methods were used. Parametric methods (*t* test) were used for evaluation, and values of *p* less than 0.05 were considered significant (two-tailed *t* test). Data are presented as means (SD) of three individual experiments.

Conflict of Interest: The authors declare no competing financial interest.

Acknowledgment. This work was financially supported by the State High-Tech Development Plan (2012AA020804), National Natural Science Foundation of China Project (nos. 30970784 and 81171455), National Key Basic Research Program of China (MOST 973 Project 2009CB930200), and National Distinguished Young Scholars Grant (31225009) from the National Natural Science Foundation of China and Chinese Academy of Sciences (CAS) "Hundred Talents Program" (07165111ZX), and the authors also appreciate the support from the "Strategic Priority Research Program" of the Chinese Academy of Sciences, grant no. XDA09030301. We sincerely thank Dr. Bhargavi Mazinder Boruah, Laboratory of Pathogenic Microbiology and Immunology, Institute of Microbiology, Chinese Academy of Sciences, for her help and valuable suggestions during preparation of the manuscript.

Supporting Information Available: Scheme and method for the synthesis of glutathione-stabilized gold NPs; calculation of the number and surface density of glutathione molecules per nanoparticle; zeta potential study of gold NPs before and after functionalization with drug and peptide; synthesis and characterization of platinum(IV) complex **1** and complex **2**; functionalization of NPs with targeting peptide (CRGDK) and platinum(IV) drug; X-ray photoelectron spectroscopy (XPS) study of Au@Pt(IV)+CRGDK NPs; agarose gel electrophoresis; physicochemical properties and stability of the NPs; cell toxicity study of Au@GSH and Au@CRGDK NPs; Table S1: IC_{50} values of platinum drugs and platinum-conjugated nanocarriers on PC-3 and DU145 cells; fabrication of FITC-NPs; localization study of nanocarriers in DU-145 cells; competition assay; and electrophoretic mobility shift assays. This material is available free of charge *via* the Internet at http://pubs.acs.org.

REFERENCES AND NOTES

1. Kelland, L. The Resurgence of Platinum-Based Cancer Chemotherapy. *Nat. Rev. Cancer* **2007**, *7*, 573–584.
2. Galanski, M.; Jakupec, M. A.; Keppler, B. K. Update of the Preclinical Situation of Anticancer Platinum Complexes: Novel Design Strategies and Innovative Analytical Approaches. *Curr. Med. Chem.* **2005**, *12*, 2075–2094.
3. Reedijk, J. New Clues for Platinum Antitumor Chemistry: Kinetically Controlled Metal Binding to DNA. *Proc. Natl. Acad. Sci. U.S.A.* **2003**, *100*, 3611–3616.
4. Chin, C. F.; Tian, Q.; Setyawati, M. I.; Fang, W. R.; Tan, E. S. Q.; Leong, D. T.; Ang, W. H. Tuning the Activity of Platinum(IV) Anticancer Complexes through Asymmetric Acylation. *J. Med. Chem.* **2012**, *55*, 7571–7582.
5. Reithofer, M.; Galanski, M.; Roller, A.; Keppler, B. K. An Entry to Novel Platinum Complexes: Carboxylation of Dihydroxoplatinum(IV) Complexes with Succinic Anhydride and Subsequent Derivatization. *Eur. J. Inorg. Chem.* **2006**, *13*, 2612–2617.
6. Reithofer, M. R.; Bytzek, A. K.; Valiahdi, S. M.; Kowol, C. R.; Groessl, M.; Hartinger, C. G.; Jakupec, M. A.; Galanski, M.; Keppler, B. K. Tuning of Lipophilicity and Cytotoxic Potency by Structural Variation of Anticancer Platinum(IV) Complexes. *J. Inorg. Biochem.* **2011**, *105*, 46–51.
7. Hall, M. D.; Hambley, T. W. Platinum(IV) Antitumour Compounds: Their Bioinorganic Chemistry. *Coord. Chem. Rev.* **2002**, *232*, 49–67.
8. Graf, N.; Bielenberg, D. R.; Kolishetti, N.; Muus, C.; Banyard, J.; Farokhzad, O. C.; Lippard, S. J. αVβ3 Integrin-Targeted PLGA-PEG Nanoparticles for Enhanced Anti-tumor Efficacy of a Pt(IV) Prodrug. *ACS Nano* **2012**, *6*, 4530–4539.
9. Xiao, H.; Qi, R.; Liu, S.; Hu, X.; Duan, T.; Zheng, Y.; Huang, Y.; Jing, X. Biodegradable Polymer-Cisplatin(IV) Conjugate as a Prodrug of Cisplatin(II). *Biomaterials* **2011**, *32*, 7732–7739.
10. Kumar, A.; Zhang, X.; Liang, X.-J. Gold Nanoparticles: Emerging Paradigm for Targeted Drug Delivery System. *Biotechnol. Adv.* **2013**, *31*, 593–606.
11. Ruoslahti, E.; Bhatia, S. N.; Sailor, M. J. Targeting of Drugs and Nanoparticles to Tumors. *J. Cell Biol.* **2010**, *188*, 759–768.
12. Kumar, A.; Ma, H.; Zhang, X.; Huang, K.; Jin, S.; Liu, J.; Wei, T.; Cao, W.; Zou, G.; Liang, X.-J. Gold Nanoparticles Functionalized with Therapeutic and Targeted Peptides for Cancer Treatment. *Biomaterials* **2012**, *33*, 1180–1189.
13. Dreaden, E. C.; Mackey, M. A.; Huang, X.; Kang, B.; El-Sayed, M. A. Beating Cancer in Multiple Ways Using Nanogold. *Chem. Soc. Rev.* **2011**, *40*, 3391–3404.
14. Gibson, J. D.; Khanal, B. P.; Zubarev, E. R. Paclitaxel-Functionalized Gold Nanoparticles. *J. Am. Chem. Soc.* **2007**, *129*, 11653–11661.
15. Brown, S. D.; Nativo, P.; Smith, J. A.; Stirling, D.; Edwards, P. R.; Venugopal, B.; Flint, D. J.; Plumb, J. A.; Graham, D.; Wheate, N. J. Gold Nanoparticles for the Improved Anticancer Drug Delivery of the Active Component of Oxaliplatin. *J. Am. Chem. Soc.* **2010**, *132*, 4678–4684.
16. Min, Y. Z.; Mao, C. Q.; Chen, S. M.; Ma, G. L.; Wang, J.; Liu, Y. Z. Combating the Drug Resistance of Cisplatin Using a Platinum Prodrug Based Delivery System. *Angew. Chem., Int. Ed.* **2012**, *51*, 6742–6747.
17. Wang, F.; Wang, Y. C.; Dou, S.; Xiong, M. H.; Sun, T. M.; Wang, J. Doxorubicin-Tethered Responsive Gold Nanoparticles Facilitate Intracellular Drug Delivery for Overcoming Multidrug Resistance in Cancer Cells. *ACS Nano* **2011**, *5*, 3679–3692.
18. Tamarkin, L.; Libutti, S. K.; Paciotti, G. F.; Byrnes, A. A.; Alexander, H. R.; Gannon, W. E.; Walker, M.; Seidel, G. D.; Yuldasheva, N. Phase I and Pharmacokinetic Studies of CYT-6091, A Novel PEGylated Colloidal Gold-rhTNF Nanomedicine. *Clin. Cancer Res.* **2010**, *16*, 6139–6149.
19. Thakor, A. S.; Jokerst, J.; Zavaleta, C.; Massoud, T. F.; Gambhir, S. S. Gold Nanoparticles: A Revival in Precious Metal Administration to Patients. *Nano Lett.* **2011**, *11*, 4029–4036.
20. Schroeder, A.; Heller, D. A.; Winslow, M. M.; Dahlman, J. E.; Pratt, G. W.; Langer, R.; Jacks, T.; Anderson, D. G. Treating Metastatic Cancer with Nanotechnology. *Nat. Rev. Cancer* **2012**, *12*, 39–50.
21. Wang, A. Z.; Gu, F.; Zhang, L.; Chan, J. M.; Radovic-Moreno, A.; Shaikh, M. R.; Farokhzad, O. C. Biofunctionalized Targeted Nanoparticles for Therapeutic Applications. *Expert Opin. Biol. Ther.* **2008**, *8*, 1063–1070.
22. Haspel, N.; Zanuy, D.; Nussinov, R.; Teesalu, T.; Ruoslahti, E.; Aleman, C. Binding of a C-End Rule Peptide to the Neuropilin-1 Receptor: A Molecular Modeling Approach. *Biochemistry* **2011**, *50*, 1755–1762.
23. Jubb, A. M.; Strickland, L. A.; Liu, S. D.; Mak, J.; Schmidt, M.; Koeppen, H. Neuropilin-1 Expression in Cancer and Development. *J. Pathol.* **2012**, *226*, 50–60.
24. Lambert, S.; Bouttier, M.; Vassy, R.; Seigneuret, M.; Petrow-Sadowski, C.; Janvier, S.; Heveker, N.; Ruscetti, F. W.; Perret, G.; Jones, K. S.; *et al*. HTLV-1 uses HSPG and Neuropilin-1 for Entry by Molecular Mimicry of VEGF165. *Blood* **2009**, *113*, 5176–5185.
25. Grandclement, C.; Borg, C. Neuropilins: A New Target for Cancer Therapy. *Cancers* **2011**, *3*, 1899–1928.
26. Bielenberg, D. R.; Pettaway, C. A.; Takashima, S.; Klagsbrun, M. Neuropilins in Neoplasms: Expression, Regulation, and Function. *Exp. Cell Res.* **2006**, *312*, 584–593.
27. Sugahara, K. N.; Teesalu, T.; Karmali, P. P.; Kotamraju, V. R.; Agemy, L.; Girard, O. M.; Hanahan, D.; Mattrey, R. F.; Ruoslahti, E. Tissue-Penetrating Delivery of Compounds and Nanoparticles into Tumors. *Cancer Cell* **2009**, *16*, 510–520.
28. Wei, T.; Liu, J.; Ma, H.; Cheng, Q.; Huang, Y.; Zhao, J.; Huo, S.; Xue, X.; Liang, Z.; Liang, X.-J. Functionalized Nanoscale Micelles Improve Drug Delivery for Cancer Therapy *in Vitro* and *in Vivo*. *Nano Lett.* **2013**, *13*, 2528–2534.
29. Sugahara, K. N.; Teesalu, T.; Karmali, P. P.; Kotamraju, V. R.; Agemy, L.; Greenwald, D. R.; Ruoslahti, E. Coadministration of a Tumor-Penetrating Peptide Enhances the Efficacy of Cancer Drugs. *Science* **2010**, *328*, 1031–1035.
30. Pompella, A.; Visvikis, A.; Paolicchi, A.; De Tata, V.; Casini, A. F. The Changing Faces of Glutathione, a Cellular Protagonist. *Biochem. Pharmacol.* **2003**, *66*, 1499–1503.
31. Simpson, C. A.; Salleng, K. J.; Cliffel, D. E.; Feldheim, D. L. *In Vivo* Toxicity, Biodistribution, and Clearance of Glutathione Coated Gold Nanoparticles. *Nanomedicine* **2013**, *9*, 257–263.
32. Huang, K.; Ma, H.; Liu, J.; Huo, S.; Kumar, A.; Wei, T.; Zhang, X.; Jin, S.; Gan, Y.; Wang, P. C.; *et al*. Size-Dependent Localization and Penetration of Ultrasmall Gold Nanoparticles in Cancer Cells, Multicellular Spheroids, and Tumors *in Vivo*. *ACS Nano* **2012**, *6*, 4483–4493.
33. Chithrani, B. D.; Ghazani, A. A.; Chan, W. C. W. Determining the Size and Shape Dependence of Gold Nanoparticle Uptake into Mammalian Cells. *Nano Lett.* **2006**, *6*, 662–668.
34. Kurata, T.; Tamura, T.; Sasaki, Y.; Fujii, H.; Negoro, S.; Fukuoka, M.; Saijo, N. Pharmacokinetic and Pharmacodynamic Analysis of Bis-Acetato-Ammine-Dichloro-Cyclohexylamine-Platinum(IV) (JM216) Administered Once a Day for Five Consecutive Days: A Phase I Study. *JPN J. Clin. Oncol.* **2000**, *30*, 377–384.
35. Latif, T.; Wood, L.; Connell, C.; Smith, D.; Vaughn, D.; Lebwohl, D.; Peereboom, D. Phase II Study of Oral Bis (Aceto) Ammine Dichloro (Cyclohexamine) Platinum (IV) (JM-216, BMS-182751) Given Daily X 5 in Hormone Refractory Prostate Cancer (HRPC). *Invest. New Drugs* **2005**, *23*, 79–84.
36. Dhar, S.; Daniel, W. L.; Giljohann, D. A.; Mirkin, C. A.; Lippard, S. J. Polyvalent Oligonucleotide Gold Nanoparticle Conjugates as Delivery Vehicles for Platinum(IV) Warheads. *J. Am. Chem. Soc.* **2009**, *131*, 14652–14653.
37. Dhar, S.; Gu, F. X.; Langer, R.; Farokhzad, O. C.; Lippard, S. J. Targeted Delivery of Cisplatin to Prostate Cancer Cells by Aptamer Functionalized Pt(IV) Prodrug-PLGA-PEG Nanoparticles. *Proc. Natl. Acad. Sci. U.S.A.* **2008**, *105*, 17356–17361.
38. Dhar, S.; Kolishetti, N.; Lippard, S. J.; Farokhzad, O. C. Targeted Delivery of a Cisplatin Prodrug for Safer and More Effective Prostate Cancer Therapy *in Vivo*. *Proc. Natl. Acad. Sci. U.S.A.* **2011**, *108*, 1850–1855.

39. Min, Y.; Mao, C.; Xu, D.; Wang, J.; Liu, Y. Gold Nanorods for Platinum Based Prodrug Delivery. *Chem. Commun.* **2010**, *46*, 8424–8426.
40. Ghezzi, A.; Aceto, M.; Cassino, C.; Gabano, E.; Osella, D. Uptake of Antitumor Platinum(II)-Complexes by Cancer Cells, Assayed by Inductively Coupled Plasma Mass Spectrometry (ICP-MS). *J. Inorg. Biochem.* **2004**, *98*, 73–78.
41. Jiang, W.; Kim, B. Y. S.; Rutka, J. T.; Chan, W. C. W. Nanoparticle-Mediated Cellular Response is Size-Dependent. *Nat. Nanotechnol.* **2008**, *3*, 145–150.
42. Rivera-Gil, P.; Jimenez De Aberasturi, D.; Wulf, V.; Pelaz, B.; Del Pino, P.; Zhao, Y.; De La Fuente, J. M.; Ruiz De Larramendi, I.; Rojo, T.; Liang, X.-J.; *et al*. The Challenge to Relate the Physicochemical Properties of Colloidal Nanoparticles to Their Cytotoxicity. *Acc. Chem. Res.* **2013**, *46*, 743–749.
43. Zhu, M.; Nie, G.; Meng, H.; Xia, T.; Nel, A.; Zhao, Y. Physicochemical Properties Determine Nanomaterial Cellular Uptake, Transport, and Fate. *Acc. Chem. Res.* **2013**, *46*, 622–631.
44. Dufort, S.; Sancey, L.; Coll, J.-L. Physico-Chemical Parameters that Govern Nanoparticles Fate also Dictate Rules for Their Molecular Evolution. *Adv. Drug Delivery Rev.* **2012**, *64*, 179–189.
45. Dasgupta, A. K.; Patra, H. K.; Banerjee, S.; Chaudhuri, U.; Lahiri, P. Cell Selective Response to Gold Nanoparticles. *Nanomedicine* **2007**, *3*, 111–119.
46. Pirollo, K. F.; Chang, E. H. Does a Targeting Ligand Influence Nanoparticle Tumor Localization or Uptake? *Trends Biotechnol.* **2008**, *26*, 552–558.
47. Bhattacharyya, S.; Singh, R. D.; Pagano, R.; Robertson, J. D.; Bhattacharya, R.; Mukherjee, P. Switching the Targeting Pathways of a Therapeutic Antibody by Nanodesign. *Angew. Chem., Int. Ed.* **2012**, *51*, 1563–1567.
48. Canton, I.; Battaglia, G. Endocytosis at the Nanoscale. *Chem. Soc. Rev.* **2012**, *41*, 2718–2739.
49. Ganta, S.; Devalapally, H.; Shahiwala, A.; Amiji, M. A Review of Stimuli-Responsive Nanocarriers for Drug and Gene Delivery. *J. Controlled Release* **2008**, *126*, 187–204.
50. Lagunas, V. M.; Meléndez-Zajgla, J. Nuclear Factor-Kappa B as a Resistance Factor to Platinum-Based Antineoplasic Drugs. *Met. Based Drugs* **2008**, *2008*, 576104.
51. Kim, S. B.; Kim, J. S.; Lee, J. H.; Yoon, W. J.; Lee, D. S.; Ko, M. S.; Kwon, B. S.; Choi, D. H.; Cho, H. R.; Lee, B. J.; *et al*. NF-κB Activation is Required for Cisplatin-Induced Apoptosis in Head and Neck Squamous Carcinoma Cells. *FEBS Lett.* **2006**, *580*, 311–318.
52. Kaspárková, J.; Nováková, O.; Vrána, O.; Intini, F.; Natile, G.; Brabec, V. Molecular Aspects of Antitumor Effects of a New Platinum(IV) Drug. *Mol. Pharmacol.* **2006**, *70*, 1708–1719.
53. Parrondo, R.; Pozas, D.; Reiner, T.; Rai, P.; Perez-Stable, C. NF-κB Activation Enhances Cell Death by Antimitotic Drugs in Human Prostate Cancer Cells. *Mol. Cancer* **2010**, *9*, 1–13.